PHYSICAL REVIEW B **70**, 104502 (2004)

Capacitance measurements on grain boundaries in $Y_{1-x}Ca_xBa_2Cu_3O_{7-\delta}$

J. H. T. Ransley,* P. F. McBrien, G. Burnell, E. J. Tarte, and J. E. Evetts
IRC in Superconductivity, Madingley Road, Cambridge, CB3 0HE, United Kingdom

R. R. Schulz,† C. W. Schneider, A. Schmehl, H. Bielefeldt,‡ H. Hilgenkamp,§ and J. Mannhart
Experimentalphysik VI, Centre for Electronic Correlations and Magnetism, Institute of Physics, Augsburg University, D-86135 Augsburg, Germany

(Received 20 April 2004; published 1 September 2004)

The capacitance of 24°[001] tilt calcium doped $Y_{1-x}Ca_xBa_2Cu_3O_{7-\delta}$ grain boundaries has been measured for thin films with x in the range 0.0–0.3. The capacitance was determined from the hysteresis in the *I-V* characteristic. By measuring the capacitance as a function of the voltage across the junctions it was possible to observe the contribution of both parasitic substrate capacitance and heating to the hysteresis. These effects enable the determination of the intrinsic capacitance of the grain boundaries. The effect of thermal noise on the measurement is also assessed, and found to be much less than the observed changes in the capacitance. The capacitance is found to increase as the calcium doping increases: from 0.2 Fm^{-2} for $x=0.0$ to a maximum of 1.2 Fm^{-2} for $x=0.3$. The changes in the capacitance per unit area are observed to be inversely proportional to the corresponding changes in the resistance area product.

DOI: 10.1103/PhysRevB.70.104502 PACS number(s): 74.72.Bk, 85.25.Cp, 73.40.Gk

I. INTRODUCTION

Shortly after the discovery of high temperature superconductors, grain boundaries were identified as the limiting factor determining the critical current in bulk samples.[1] Since then there has been a major effort to increase the grain boundary critical currents in these materials.[2] Recently it has been demonstrated that improvement in the critical currents attainable in the technologically promising superconductor $YBa_2Cu_3O_{7-\delta}$ can be achieved by doping the grain boundaries with calcium.[3–5] If grain boundary critical currents are to be further increased, a better understanding of the mechanisms by which calcium alters the grain boundary properties is needed. Presently it is thought that the calcium alters the carrier density and the amount of trapped charge at the boundary, changing the form of the potential barrier.[6] There is increasing evidence from transmission electron microscopy that the width and voltage of the potential barrier at the grain boundary are reduced by calcium doping.[7] By measuring the capacitance of the grain boundary it is possible to obtain information on the width of the barrier that is independent of the barrier voltage.

In previous experiments the capacitance of high angle, Josephson coupled, grain boundaries has been measured by considering the hysteresis in current-voltage curves and by measuring the voltages of Fiske resonances present in the junction.[8–16] In this work we measure the capacitance of a series of thin film $Y_{1-x}Ca_xBa_2Cu_3O_{7-\delta}$ grain boundaries. Capacitance as a function of doping was determined from hysteresis in the current-voltage characteristics of Josephson junctions fabricated from the thin films. Particular care has been taken to eliminate possible sources of systematic error from the measurement. It is necessary to ensure that the capacitance measured is that of the grain boundary alone, and that there is not a large parasitic contribution from the $SrTiO_3$ substrate.[16] It is important to show that the measured hysteresis is neither significantly increased by heating effects[17] (heating can induce hysteresis in junctions that have no capacitance) nor reduced by the effect of the thermal noise[18] (which leads to premature switching into and out of the superconducting state).

In addition to the capacitances, the normal resistances and the critical currents of the boundaries were measured. The capacitance values were compared with these transport properties and with the structural features of the boundary, in order to gain insight into the nature of calcium doping.

II. METHODS

Epitaxial thin films were deposited by pulsed laser deposition from polycrystalline $Y_{1-x}Ca_xBa_2Cu_3O_{7-\delta}$ targets onto 24°[001] tilt $SrTiO_3$ bicrystal substrates. Five films were grown: one for each of the dopings $x=0.0$, $x=0.1$, $x=0.2$, and two with doping $x=0.3$. Film thicknesses were measured by AFM on wet etched steps and were in the range 120–180 nm. Microbridges across the grain boundaries were patterned by standard photolithography and argon ion milling. The widths of the bridges were between 2 μm and 6 μm, as measured by optical microscopy. Current biased current-voltage characteristics were measured by the standard four point technique, with the sample immersed in liquid helium or in helium vapor, at atmospheric pressure. Figure 1 shows a series of current density-voltage characteristics for the 3 μm junctions, as well as the detail of the hysteresis for the 30% calcium doped 3 μm junction. The critical current criterion adopted was a significant increase above the noise level (typically 1 μV). The same criterion was used to define the return currents. Normal resistances were obtained from current-voltage characteristics with large applied bias, such as those shown in Fig. 1(a).

III. DETERMINING THE INTRINSIC CAPACITANCE OF THE GRAIN BOUNDARIES

The capacitance of the grain boundaries can be measured by taking advantage of the Josephson coupling that occurs

 ©2004 The American Physical Society

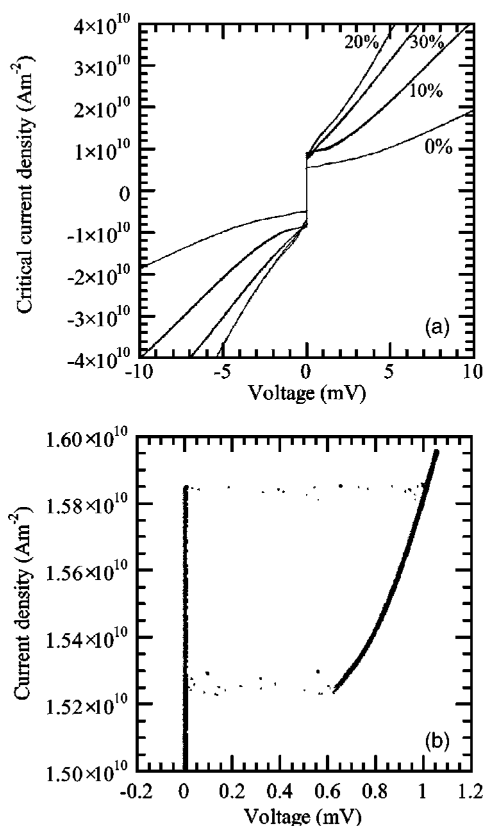

FIG. 1. (a) Current density-voltage characteristics for 3 μm wide junctions of each of the 3 dopings, measured at 4.2 K with the sample immersed in liquid helium. (b) Detail of the hysteresis for the 30% doped 2 μm wide junction. Ten consecutive measurements are shown to give an indication of the noise level.

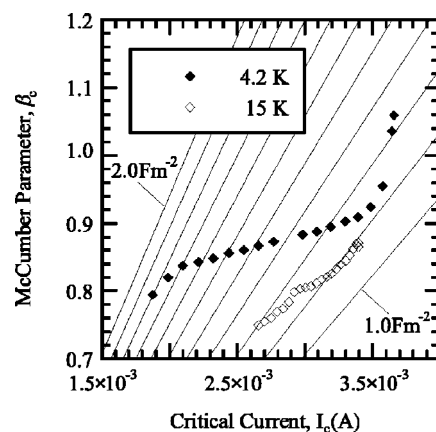

FIG. 2. Plot of the McCumber parameter, β_c, against the critical current, I_c for the 30% calcium doped 2 μm junction at two different temperatures. Equation (1) predicts a linear relationship between β_c and I_c for a constant capacitance. Lines of constant capacitance per unit area, spaced at intervals of 0.1 Fm^{-2} are also shown.

across them. Josephson junction capacitances can be determined from values of the return current and the critical current extracted from current-voltage characteristics such as those shown in Fig. 1(b). Within the resistively and capacitively shunted junction (RCSJ) model it is possible to determine the McCumber parameter, β_c, from the ratio of the critical current, I_c, to the return current, I_r, using the numerical result of McCumber.[19] β_c is in turn related to the capacitance by the following equation:

$$\beta_c = \frac{2eI_cR_n^2C}{\hbar}, \quad (1)$$

where e is the electronic charge, $\hbar$ is Planck's constant divided by 2π, R_n is the normal resistance of the junction, and C is its capacitance.

This equation predicts a linear relationship between β_c and I_c given that all the other parameters are constant. It is possible to suppress the critical current of a junction by applying a dc magnetic field in the junction plane so the relationship between β_c and I_c can be measured experimentally. Figure 2 shows such a relationship for one of the grain boundary junctions measured in this study. It is clear that the relationship between these two quantities is not linear for this device at either 4.2 K or 15 K. As expected, the normal resistance is found to be independent of the applied magnetic field and therefore the capacitance must be increasing at lower critical currents or the hysteresis must be due to some other effect.

The reduction of the critical current by the application of a magnetic field results in a reduction of the return voltage at which the junction switches back into the superconducting state. In the finite voltage state the current flowing through the junction resistance and capacitance oscillates at a frequency proportional to the time averaged dc voltage. So reducing the critical current also has the effect of reducing the frequency of the Josephson oscillations at the return current (which is also reduced). The dielectric properties of the $SrTiO_3$ substrate are frequency dependent and at lower frequencies the relative dielectric constant can be extremely large. It is therefore possible that a parasitic capacitance is added to the system at lower voltages as electric field is diverted into the high dielectric constant substrate. This situation is illustrated in Fig. 3(a). As shown in Fig. 3(b), the dielectric constant of $SrTiO_3$ is a function of both frequency and temperature.[20] The Josephson voltages equivalent to the frequencies are shown as an alternative x-axis in Fig. 3(b). It is clear that in the 0–1 mV voltage range the parasitic capacitance is likely to increase at lower voltages (and hence reduced critical currents).

A second possible explanation for the nonlinear curves observed in Fig. 2 is that the hysteresis observed is dominated by heating.[17] Self-heating of the junction can cause a reduction in the measured return current and can lead to hysteresis even in the absence of capacitance. To understand this effect consider traversing a single hysteresis loop in the *I-V* curve. As the current is initially increased the sample is in the superconducting state and there is no dissipation or heating. Once the sample switches into the normal state there is a voltage across the junction and power is dissipated as heat. The junction temperature rises. Provided this rise in temperature is significant there will be a corresponding decrease in the critical current. The junction will switch back at the reduced critical current, appropriate for its increased tempera-

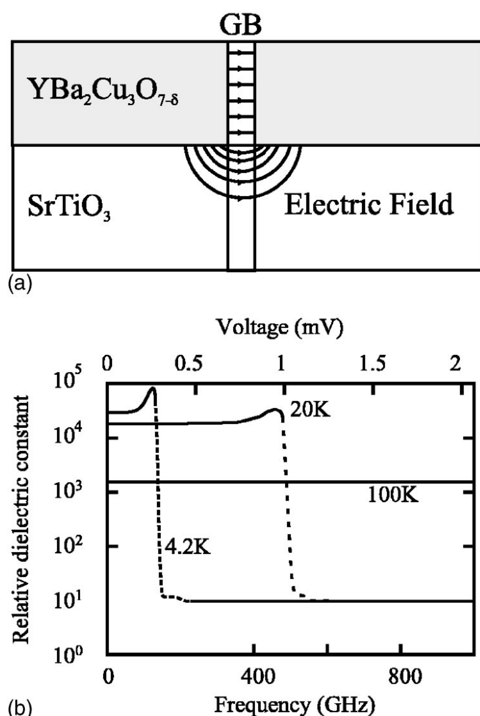

FIG. 3. (a) Diagram illustrating the effect of a large substrate capacitance on the electric field distribution in the vicinity of the grain boundary. The substrate contributes parasitically to the overall capacitance. (b) Schematic temperature and frequency dependence of the dielectric constant of single domain $SrTiO_3$. The equivalent Josephson voltage for a given frequency is shown as an alternative x-axis (based on Neville, Hoeneisen, and Mead, Ref. [20]).

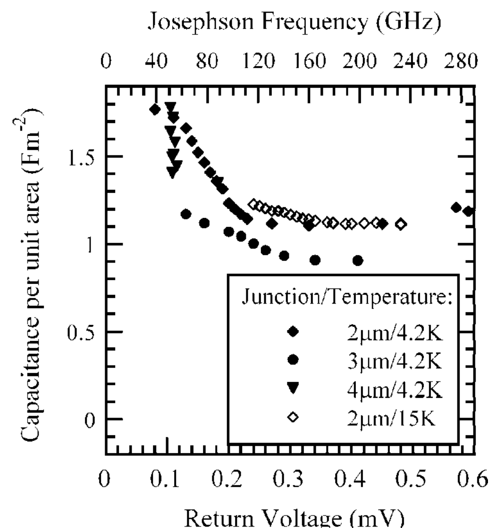

FIG. 4. Measured capacitance per unit area, C/A, shown against the return voltage. At 4.2 K the sample is immersed in liquid helium, at 15 K it is held in helium vapor. The Josephson frequency is shown as an alternative x-axis and is effectively the frequency at which the capacitance is measured. The sharp rise in the capacitance at low frequencies is due to parasitic components from the substrate. At higher frequencies the capacitance is constant and temperature independent.

ture. For junctions that are already hysteretic heating effects will increase the amount of hysteresis.

Finally there is the possibility that the hysteresis is suppressed by thermal noise in the junction, which leads to switching out of the superconducting state at a reduced current and switching back at an increased current. While this cannot explain the results of Fig. 2 it is nonetheless important to assess its effect on the measurement as it is likely to be a major source of error.

The effects of both the substrate and heating must be ruled out in any measurement of the grain boundary capacitance and the error due to thermal noise should be estimated. In the remainder of this section the experiments performed to ensure that the measured capacitance is that intrinsic to the grain boundary and to assess the effect of thermal noise are described.

A. Eliminating substrate effects from the capacitance measurement

To rule out substrate effects it is necessary to demonstrate that the junction properties are measured at a sufficiently large frequency that the dielectric constant of the substrate is low. The detailed behavior of the dielectric constant of $SrTiO_3$ is shown schematically in Fig. 3(b). At 4.2 K and at low frequencies the relative dielectric constant (ε_r) is very high (approximately 20 000). ε_r remains high until the soft optic phonon frequency, ν_{so}, is reached. At this point there is a rapid drop in ε_r with increasing frequency and at high frequencies $\varepsilon_r \approx 10$. As the temperature is increased the zero frequency value of ε_r is reduced, whilst ν_{so} increases, but similar behavior is observed. The location of the sharp drop in the dielectric constant is also dependent on the domain structure in the $SrTiO_3$, which forms as the sample is cooled below 110 K,[21] so the diagram is necessarily a schematic representation of the behavior of the substrate.

If the substrate does cause the variations in capacitance shown in Fig. 2, then it should be possible to observe voltage (effectively frequency) and temperature dependencies of the capacitance that reflect the behavior of the dielectric constant. Figure 4 shows the data from Fig. 2 plotted in an alternative manner, as capacitance versus return voltage. The return voltage is the appropriate voltage for the retrapping process and so reflects the frequency at which the capacitance is measured, shown as an alternative x-axis. In addition to the data from the 30% calcium doped, 2 μm junction, results from other devices on the same sample are also shown. A sharp increase in the capacitance at low frequencies is apparent for all the junctions and in addition occurs at the same frequency as the sharp rise in the dielectric constant of $SrTiO_3$ (see Fig. 3). At larger voltages and hence frequencies the capacitance of both the 2 and 3 μm junctions levels out to a constant value, indicative of a negligible substrate contribution. The same behavior was observed from an additional 5 μm junction on the same sample. The capacitance of the 4 μm junction varies continuously over the measurable range so there is always some substrate capacitance. It is therefore not possible to measure the grain boundary capacitance of this junction by this technique. The high frequency capacitance of the 2 μm junction measured at 15 K is the

same as the 4.2 K value, in very different thermal conditions. The onset of the increase in the capacitance due to parasitic substrate contributions occurs at a higher frequency at 15 K than at 4.2 K. The magnitude of the parasitic contributions is also reduced, as expected from Fig. 3(b). The data in Fig. 4 are therefore convincing evidence that the substrate effect on the measurement can be both observed and eliminated.

This consistency of the results in Fig. 4 with the behavior of the substrate shown in Fig. 3(b) enables us to be confident that we observe the effects of the substrate on the measurement. Other authors have observed similar, enhanced grain boundary capacitances in hysteresis[11] and Fiske resonance[9,11] measurements of $YBa_2Cu_3O_{7-\delta}$ (on $SrTiO_3$) grain boundary capacitance at low frequencies. Nakajima, Yokota, Myoren, Chen, and Yamashita confirmed that this effect was due to the substrate capacitance by demonstrating a large electric field effect.[11] Tarte *et al.* have observed a transition in the capacitance of $YBa_2Cu_3O_{7-\delta}$ grain boundaries on $SrTiO_3$ at a voltage of 0.25 mV (equivalent to a frequency of 130 GHz), by observations of the Fiske resonance dispersion relation.[15] Their results are discussed in more detail below. The parasitic substrate contribution to the capacitance can be eliminated by measuring the capacitance in the high frequency region. Notice that the measured capacitance of the 2 μm junction at the highest return voltages is slightly increased. This increase is not observed in the same junction at 15 K and may result from the onset of heating effects. The effect of heating on the measurement is assessed in more detail below.

Fiske resonances have been frequently used to determine the capacitance of $YBa_2Cu_3O_{7-\delta}$ grain boundaries.[8–11,16] The voltage (V_n) at which an nth order Fiske resonance occurs is given by

$$V_n = \frac{n\Phi_0}{2l\sqrt{L'C'}}, \tag{2}$$

where Φ_0 is the flux quantum, l is the width of the junction, and L' and C' are the inductance and capacitance, per unit length of the junction. An nth order Fiske resonance corresponds to a cavity resonance in which $n/2$ wavelengths fit into the junction cavity.

Using Eq. (2), the inductance per unit length of the junction can be determined from the Fiske resonance voltage. If the inductance of the junction is dominated by the superconducting electrodes, then the value of the inductance can be simply related to the London penetration depth.[16] By plotting the Fiske resonance voltage against the inverse junction width (effectively a dispersion relation for the junction cavity) the junction inductance can be determined from the gradient if the capacitance is known from the hysteresis. Figure 5 shows a plot of data from several undoped junctions from the literature, together with the data obtained from the 30% doped junction. It is clear that the dispersion relation for the undoped data has two linear regimes—one at low voltages (below 0.3 mV) and one at high voltages (above 0.3 mV). Analysis of the data in the high voltage regime produces a reasonable penetration depth of 180 nm for the junction region.[16] The lower voltage regime, however, has an increased gradient and does not produce a consistent penetration depth. This is because the dielectric constant of the substrate is extremely large at these reduced voltages (and hence reduced Josephson frequencies) and substrate effects alter the current distribution in the superconducting electrodes increasing both the inductance and capacitance per unit length of the junction [see Fig. 3(b)].

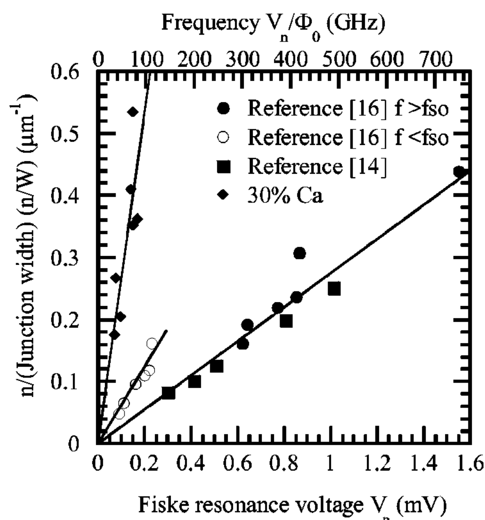

FIG. 5. Fiske resonance dispersion relations for undoped junctions from Tarte *et al.* (Ref. 15) and for the 30% doped junctions from this study.

It is clear that the data obtained for the 30% doped sample are all in this low frequency, substrate dominated, region. Although this implies that a quantitative analysis of the Fiske resonances is not possible, qualitative observations can be made. The gradient of the curve for the 30% doped sample is approximately 5 times greater than that previously observed for an undoped sample in the same low frequency regime. This is consistent with a significant increase of the junction capacitance. The fact that the resonances occur at such low voltages is a further indication of an increased capacitance and is consistent with the observations from the hysteresis measurements.

In addition to measuring the frequency dependence of the capacitance by suppressing the critical current with a magnetic field, the temperature dependence of the zero field capacitance was measured. The data from this experiment are shown in Fig. 6. The variation of the return voltage with temperature is also shown. In general the return voltage decreases as the temperature increases, since at higher temperatures the critical current is reduced. It is clear that in most cases the capacitance is approximately temperature-independent over the measurable range. At 4.2 K the return voltages of all the samples, with the exception of the 3 μm 30% doped junction, are out of the substrate dominated regime—determined from Fig. 4. The effect of the substrate for this junction is to cause a rise in the capacitance, since as the temperature is increased the location of the drop in the substrate dielectric constant moves up in frequency and the return voltage drops further into the substrate dominated regime. The decreasing capacitance of the 2 μm junction may be associated with heating effects at low temperatures caus-

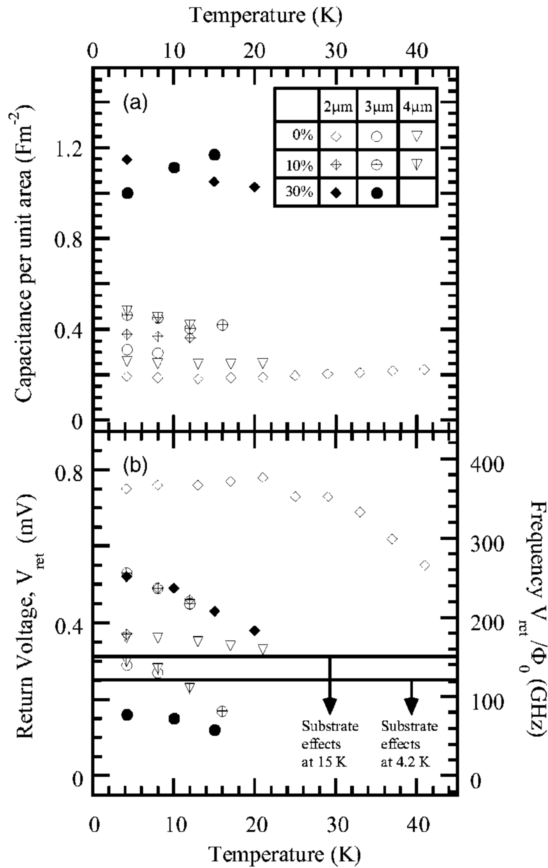

FIG. 6. (a) Temperature dependence of the zero field capacitance of a number of junctions in the study. The capacitance is determined from the hysteresis in the *I*-*V* curve with the sample in helium vapor, or immersed in liquid helium at 4.2 K. In most cases the capacitance is independent of temperature to within the error associated with the measurement (approximately 10% if the systematic errors are ignored). (b) Return voltage of these junctions as a function of temperature. With the exception of the 3 μm 30% calcium doped junction the return voltages are all above the substrate dominated regime at 4.2 K.

ing an artificially inflated low temperature capacitance value. The temperature independence of the 2 μm undoped junction capacitance provides further evidence that the technique is consistent—a temperature independent capacitance would not be observed up to 40 K if the measured capacitance were dominated by the substrate or if the hysteresis were caused by heating. The effect of heating is assessed in more detail in the next part of this section.

B. Eliminating heating effects

The previous discussion highlighted the possibility that heating may contribute significantly to the measured hysteresis. In order to investigate this possibility we have developed a detailed model for heating in the high-T_c grain boundary. This model is described in full in the Appendix. By adapting the model of Skocpol, Beasley, and Tinkham[17] to the geometry of bicrystal grain boundaries we are able to calculate the temperature rise expected at any point in the *I*-*V* curve.

TABLE I. Temperature rise associated with heating of the junction in the normal state at the return current, ΔT_{ret}, and at the critical current, ΔT_{crit}. Values are calculated for different values of x in $Y_{1-x}Ca_xBa_2Cu_3O_{7-\delta}$, different junction widths w and different temperatures, T. The return voltage, V_{ret}, is also shown for easy comparison with Fig. 4. The calculations were performed using the model outlined in the Appendix. Note that the predicted temperature increase is approximately the same for all the junctions in the study and that it is strongly reduced as the temperature is increased.

x	w (μm)	T (K)	V_{ret} (mV)	ΔT_{crit} (K)	ΔT_{ret} (K)
0	4	4.2	0.6	1.0	0.9
0	3	4.2	0.5	1.0	0.7
0	2	4.2	0.7	1.7	1.0
10	4	4.2	0.3	0.9	0.7
10	3	4.2	0.6	1.9	1.3
10	2	4.2	0.4	0.9	0.8
30	5	4.2	0.2	0.6	0.5
30	4	4.2	0.1	0.5	0.4
30	3	4.2	0.2	0.7	0.6
30	2	4.2	0.6	2.3	1.6
30	2	15.0	0.5	0.3	0.2

Table I shows the temperature increases for all the hysteretic junctions measured in this study, calculated for key points on the *I*-*V* curve. The power dissipated in these junctions typically leads to temperature increases of the order of 1 K at the return current. For the junctions measured in this study the critical current is found to be temperature independent at low temperatures, so small variations in temperature are unlikely to make a significant difference to the hysteresis.

The expected hysteresis $(\alpha = I_{ret}/I_c)$ due to a small temperature rise at the junction is $\alpha = 1 + (\Delta T/I_c) \times dI_c/dT$. A typical value for $1/I_c \times dI_c/dT$ is -3×10^{-3} K^{-1} for an optimally doped 24°[001] tilt $YBa_2Cu_3O_{7-\delta}$ grain boundary.[2] For temperature rises of order 1 K this leads to $\alpha = 0.997$, which should be compared to the measured values in this study, in the range 0.95–0.995. The temperature increases associated with heating in the 2 μm 30% calcium doped junction are the largest. This was the junction in which heating effects were expected from the rise in the capacitance observed at high return voltages in Fig. 4 and the temperature dependence of the capacitance in Fig. 6. The observation of the onset of heating effects in this junction gives us confidence that such effects do not occur in the other junctions, in which less power is dissipated at the return current. In the case of this junction the capacitance could be extracted from measurements at 15 K, where the heating is significantly reduced. In addition most of the junctions measured in this study had a temperature independent capacitance, as shown in Fig. 6. The observation of a temperature independent capacitance suggests that heating effects are negligible—it is clear from the data in Table I that the effects of heating are strongly reduced at higher temperatures.

Heating effects can therefore be eliminated by careful consideration of the temperature and magnetic field dependence of the critical current. A self-consistent picture

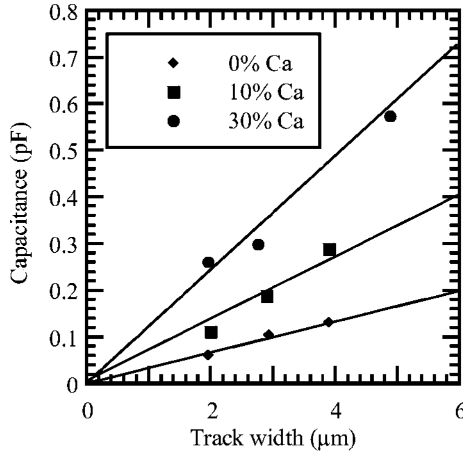

FIG. 7. Junction capacitance at 4.2 K shown against width of the device for the different samples measured. The straight lines serve as a guide to the eye.

emerges from these measurements and indicates that it is possible to measure the grain boundary capacitance using the junction hysteresis. Further evidence for the consistency of the technique comes from the scaling of the measured capacitance with junction width, shown in Fig. 7. Having demonstrated that the capacitance measured is due to the grain boundary itself, the next section assesses the systematic effect of thermal noise on the measured hysteresis.

C. The effect of thermal noise on the measured capacitance

Thermal or other noise sources cause a reduction in the measured critical current and an increase in the return current, producing a systematic underestimate of the capacitance. The washboard analogue for the resistively and capacitively shunted Josephson junction provides a simple explanation for this effect.[22] In the presence of a noise source the superconducting state becomes metastable at currents just below the critical current, when the size of the washboard potential well becomes comparable to kT (where k is Boltzmann's constant and T is the noise temperature). The junction switches into the normal state prematurely as a result of noise excitation out of the potential well. Similarly the return process can occur at currents greater than the return current, with the noise source leading to premature retrapping into the washboard potential well. As a consequence of the noise the junction does not switch out at a fixed current, but rather the observed critical currents are distributed across a finite range of currents. By measuring the distribution of the observed critical currents it is possible to determine the lifetime of the states corresponding to the observed currents.[18]

Kramers[23] showed that in the intermediately damped (or the transition state) regime the lifetime, τ, of the state corresponding to a current just below the critical current is given by

$$\tau^{-1} = \frac{\omega}{2\pi}\exp\left(-\frac{E}{kT}\right), \tag{3}$$

where $\omega/2\pi$ is the frequency of escape attempts from the potential well, E is the energy of the washboard potential barrier, k is Boltzmann's constant, and T is the temperature. For a Josephson junction tilted washboard the values of E and ω are

$$E = \frac{I_c\phi_0}{\pi}\left(\sqrt{1-\left(\frac{I}{I_c}\right)^2} - \frac{I}{I_c}\arccos\left(\frac{I}{I_c}\right)\right), \tag{4}$$

$$\omega = \left(\frac{2\pi I_c}{\phi_0 C}\right)^{1/2}\left(1-\left(\frac{I}{I_c}\right)^2\right)^{1/4}, \tag{5}$$

where I is the current of the metastable state, I_c is the true (zero noise) critical current, C is the junction capacitance and Φ_0 is the flux quantum. The assumptions implicit in the above analysis are that $\omega\tau \gg 1$ and that $E/kT > RC\omega > 0.8$. The junctions in this work satisfy these requirements.

To calculate the inverse lifetime of a given current state, the critical current data are reduced to the form of a histogram with N current bins. The lifetime of the state corresponding to each current bin, $\tau^{-1}(K)$ (where $K=1,\ldots,N$) can then be determined. We denote $K=1$ as the current bin with largest critical current and $K=N$ as that with the smallest. Fulton and Dunkleberger showed that $\tau^{-1}(K)$ is given by[18]

$$\tau^{-1}(K) = \frac{dI}{dt}\frac{1}{\Delta I}\ln\left(\frac{\Sigma_{j=1}^{K}P(j)}{\Sigma_{i=1}^{K-1}P(i)}\right), \tag{6}$$

where dI/dt is the current sweep rate at the Kth current bin, ΔI is the width of the current bin and $P(i)$ is the number of switching events that occur within the ith current bin. In deriving this equation it is assumed that $\dot{I}/I_c \ll \omega, \tau^{-1}$ and that the current applied can be approximated as increasing linearly with time over the period corresponding to a single current interval. Again these approximations are valid for our experimental conditions.

Having calculated τ^{-1} for a number of current intervals it is possible to produce a plot of $\ln(2\pi\tau^{-1}/\omega)$ versus E/k, provided a value for the true (zero noise) critical current, I_c, is assumed. Initially this is fixed at the value of the largest critical current observed. From Eq. (3) it is clear that such a graph should have an intercept of zero and a gradient of $1/T$, where T is the noise temperature. The value of I_c is increased until the condition of zero intercept for the graph is satisfied. In this way the true critical current is determined and the noise temperature can also be extracted from the gradient of the graph.

Figure 8(a) shows the distribution of critical currents obtained for the 2 μm 30% Ca doped junction, together with the theoretical distribution obtained from the above analysis. Figure 8(b) shows the plot of $\ln(2\pi\tau^{-1}/\omega)$ versus E/k that was used to calculate the true critical current and the noise temperature. For these data the noise temperature is 54 K, significantly above the measurement temperature of 4.2 K. The most likely cause of the excess noise is Johnson noise transmitted down the wires in the measurement probe to the device. Indeed in previous experiments to measure critical current distributions special precautions had to be adopted to prevent this.[18,24] The bandwidth of this measurement (effectively the inverse total measurement time to the attempt frequency ω) is sufficiently large that the contribution of $1/f$

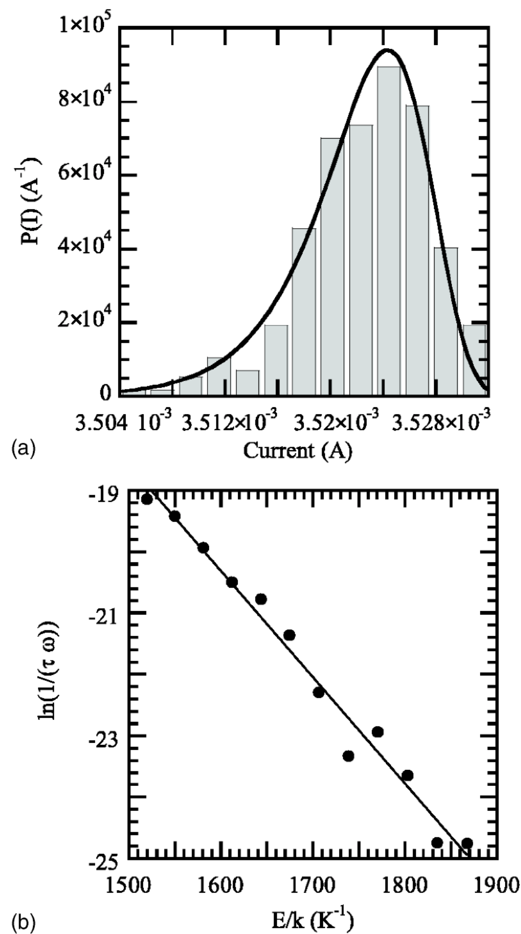

FIG. 8. (a) Distribution of critical currents for the 30% doped 2 μm junction at 4.2 K. The continuous line shows a fit corresponding to a noise temperature of 54 K. (b) $\ln(1/\omega\tau)$ versus E/k [see Eq. (3)]. The gradient of this graph is used to extract the noise temperature of the measurement and the condition of zero intercept can be used to extract the zero noise critical current. The linear relationship indicates a thermal distribution.

noise to the switching distribution is expected to be negligible in comparison to the white noise. The fact that Fig. 8(b) is linear indicates that the noise is frequency independent, so the above analysis is applicable. The value of the true critical current was found to be 3.67 mA, so the value measured is approximately 4% lower than the true value. The effect of this systematic underestimate is discussed below.

The return currents can also be treated by a similar analysis to estimate the effect of the noise.[25,26] Generally the return currents are less susceptible to thermal noise than the critical currents,[22] so it is more difficult to measure their distribution. The 2 μm 30% Ca doped junction was found to have a nonthermal current distribution. A possible cause of this problem is that shot noise makes a significant contribution to the noise across the junction. Likharev identifies the limit at which shot noise becomes important as voltages above 0.5 mV at 4.2 K.[22] This is comparable to the return voltage across the junction when it switches back (0.48 mV in zero field).

If we assume that the effect of the noise on the return current is comparable to its effect on the critical current (i.e., the measured return current is 4% above the true return current) we can estimate the systematic error in the capacitance. This assumption will overestimate the effect of noise on the measurement, since the critical current distribution is generally broader than the return current distribution for a given noise temperature. The 4% errors in both the critical and return current translate to a 25% systematic underestimate of the capacitance. While this is significant, it is much less than the 500% increases in the capacitance we observe as the calcium doping is increased from 0% to 30% (see Fig. 9). The error is also consistent, because the capacitance of the junctions scales well with the track width (see Fig. 7) and is approximately temperature independent (see Fig. 6). This consistency occurs because the noise temperature is larger than the measurement temperature in all cases and indicates that the noise is fundamental to our measurement apparatus.

Thermal noise therefore produces a significant, but consistent underestimate of the capacitance. The measured capacitance is likely to be approximately 75% of the true value in the absence of thermal noise. This is significantly less than the 500% increase in the capacitance observed as the Ca doping is changed.

In summary, measurements of the junction capacitance from the current-voltage hysteresis demonstrate that the capacitance is dominated by the substrate at low frequencies. By measuring the capacitance at higher frequencies the intrinsic grain boundary capacitance can be determined. Figure 4 demonstrates the absence of substrate effects at higher return voltages (equivalently at higher measurement frequencies). The results obtained from hysteresis measurements on the 30% calcium doped junctions are in qualitative agreement with the data from Fiske resonances, although the resonances themselves all occur in the low frequency, substrate dominated regime and so cannot be used to extract the capacitance. The temperature dependence of the capacitance was measured for all the junctions in this study. For the undoped 2 μm wide junction the capacitance was measured up to 40 K and was found to be temperature independent, this is further evidence that the technique is viable. There was some indication that heating may be significant, particularly in the case of the 30% calcium doped 2 μm junction which had the highest critical current density of all the junctions measured in this study. Calculations of the temperature rises associated with heating of the junctions revealed that this junction had the largest heating effect. A self-consistent picture emerges from these measurements and indicates that it is possible to measure the grain boundary capacitance using the junction hysteresis. The major error associated with this technique is due to suppression of the junction hysteresis by thermal noise. The effect of thermal noise can be estimated by measuring the distribution of critical currents obtained from sequential measurements. Such a measurement demonstrates that thermal noise produces a systematic underestimate of the capacitance of approximately 25%, which is much less than the 500% increase in the capacitance observed in the next section. Figure 4 shows that the effect of thermal noise is temperature independent. It also demonstrates that at large return voltages the substrate effect is negligible and that heating is not a significant problem, except at the largest return voltages.

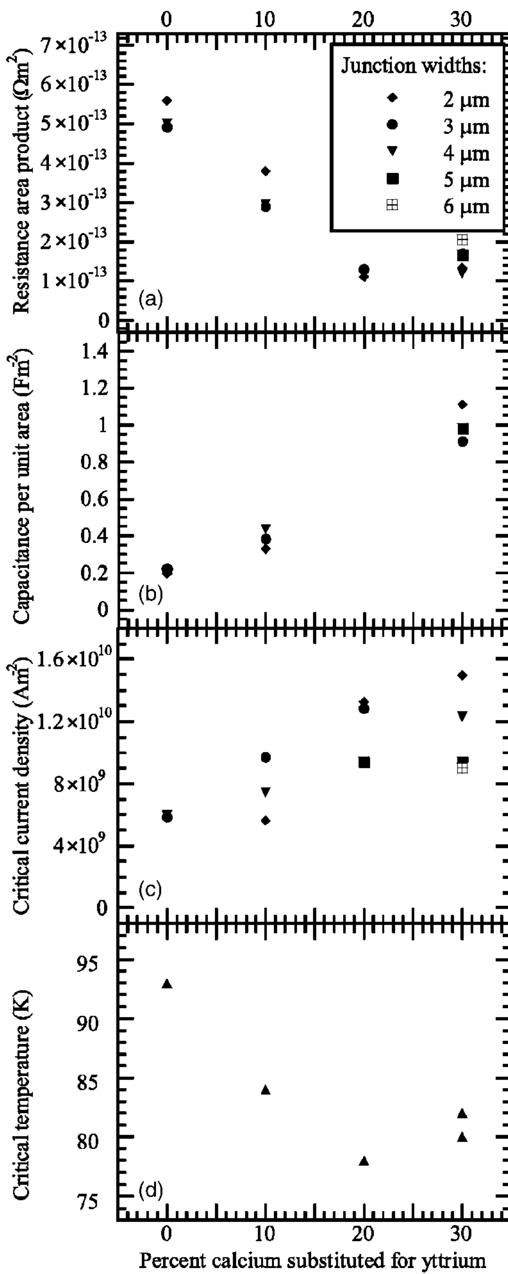

FIG. 9. Dependence of (a) the normal resistance area product, (b) the capacitance per unit area, (c) the critical current density, and (d) the critical temperature, on the amount of calcium doping. (a)–(c) were measured with the samples immersed in liquid helium at atmospheric pressure. The different symbols correspond to junctions of different widths. Experimental errors are approximately 15% of the measured value in (a) and (c) and 1 K in (d). The errors in (b) are discussed in more detail in Secs. III and IV.

IV. CAPACITANCE AS A FUNCTION OF DOPING

Figure 9 shows the transport and normal state properties of the films measured at 4.2 K, together with the capacitance, as measured by the junction hysteresis. The previous discussion has demonstrated that both heating and parasitic substrate capacitances do not effect the results. The effect of thermal noise is that the measured capacitances are approximately 25% less than the true values, and this should be considered when interpreting the results. Note also that there are further systematic errors associated with the accuracy of measuring the size of the tracks and the film thickness. Together with the random errors associated with determining the return current and the critical current, these errors amount to approximately 15% of the measured capacitance values.

There is a clear trend of increasing capacitance per unit area, decreasing resistance-area product and increasing critical current density as the calcium doping in the films is increased. The results, including the scatter in the data, are consistent with the previous work by Schneider *et al.*[4] The capacitance of the junctions increases from 0.2 Fm^{-2} for the undoped sample to a maximum value of 1.2 Fm^{-2} for the 30% doped sample. Note that there are no capacitance measurements for the 20% doped sample since none of the junctions on this sample were hysteretic.

V. DISCUSSION

The measured values of the grain boundary capacitance for doped and undoped samples can now be compared with the other properties of the boundaries—to gain further insight into their nature.

The undoped boundaries had a capacitance of 0.2 Fm^{-2}, similar to the value of 0.1 Fm^{-2} predicted by Mannhart and Hilgenkamp using the band bending model.[6] We use a similar approach to consider the results from the undoped film. The capacitance per unit area, C/A, is related to the barrier thickness, t, by the simple relation: $C/A=(\varepsilon_r\varepsilon_0)/t$, where ε_r is the relative dielectric constant, and ε_0 is the permittivity of free space. The barrier thickness, t, is made up of two depletion regions, width l_d, and the structural width of the boundary, $d(t=2l_d+d)$. d has been measured by TEM and was found to be a few atomic spacings.[27,28] We take $d\approx 0.2$ nm and assume $\varepsilon_r \approx 20$, a value well within the range of values for the dielectric constant in the literature.[6] The capacitance per unit area measured in this study for undoped boundaries is 0.2 Fm^{-2}. Assuming a uniform barrier, it is possible to calculate the width of the depletion region: $l_d=0.3$ nm. The built in voltage, V_{bi}, is related to l_d by $V_{\mathrm{bi}}=l_d^2 en/2\varepsilon_0\varepsilon r$, where e is the electronic charge and n is the carrier density ($4.5\times 10^{27}\ \mathrm{m}^{-3}$ for $YBa_2Cu_3O_{7-\delta}$). Using this relation we calculate a value of $V_{\mathrm{bi}}=0.2$ V. The built in voltage and the measured capacitance enable us to calculate the charge on the boundary, which in turn enables an estimate of the number of charge trapping sites per unit area of the boundary, S_{GB}. In this case $S_{GB}=3\times 10^{17}\ \mathrm{m}^{-2}$ (using $S_{GB}=CV/eA$). This value is within an order of magnitude of that predicted by Browning on the basis of the structural unit model.[28]

A uniform boundary with a capacitance per unit area of 1.0 Fm^2 (the capacitance of the 30% doped boundaries) has a total width, t, of 0.2 nm, if ε_r is 20. However it is not possible to conclude that the Ca doping has completely eliminated the charge on the boundary (leaving just the structural width of the boundary), since the observed decrease in resistance is too small. A fourfold decrease in the width of the barrier would produce an extremely large decrease in the barrier resistance, which is exponentially dependent on the barrier width. The relationship between the resistance and

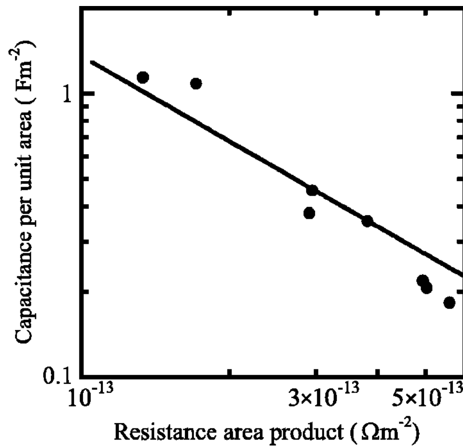

FIG. 10. Capacitance per unit area shown against resistance area product at 4.2 K for all the junctions measured in this study. The solid line shows the relation $C/A \propto 1/R_nA$.

the capacitance as the doping is varied is shown in Fig. 10. This relationship is well approximated by the following equation:

$$C/A \propto \frac{1}{R_nA}. \tag{7}$$

Such a relationship is inconsistent with a simple model of the grain boundary in which the tunnel barrier is homogenous across the width of the junction. The change in the capacitance is much too large for the observed changes in the normal state resistance. The data do not, however, rule out a tunneling model because of the extremely inhomogeneous nature of grain boundaries in $YBa_2Cu_3O_{7-\delta}$. The microstructure of grain boundaries in thin film samples is typically very complex,[29,30] with structures that include nanoscale faceting[27,31] and microscale meandering[32] of the grain boundary. The capacitance per unit area of the grain boundary scales as the inverse of the boundary thickness $(C/A =(\varepsilon_r\varepsilon_0)/t)$ whilst the resistance area product will probably scale approximately as $R_nA \propto e^{-B(t)t}$, where $B(t)$ is a tunneling parameter. The resistance area product will therefore be dominated by contributions from the narrowest regions of the barrier.[33] With inhomogeneities on many length scales it is difficult to predict the expected relationship between the normal resistance area product and the capacitance per unit area, but it is clear that the capacitance will decrease less rapidly with increasing resistance area product than a simple one-dimensional model would predict. The relationship between capacitance per unit area and resistance area product given in Eq. (7) has been observed by a number of authors with various grain boundary geometries.[16,34] Such a relationship is consistent with changes in the effective area of the boundary. This may imply that the narrowest regions of the boundary dominate both the capacitance and the normal resistance and that the proportion of these regions is increasing as calcium is added. Such a conclusion is necessarily tentative. A further complication in the interpretation of the data is that it is not clear how the addition of calcium alters the dielectric constant of the barrier region. However, it is clear that calcium doping produces a definite increase in the capacitance of the boundary.

VI. CONCLUSIONS

We have measured the capacitances of $Y_{1-x}Ca_xBa_2Cu_3O_{7-\delta}$ grain boundaries on $SrTiO_3$ substrates, with x between 0.0 and 0.3. By measuring the capacitance as a function of the return voltage we observed the effects of both parasitic substrate contributions and heating on the capacitance measurements. At 4.2 K, the substrate contributes to the capacitance at return voltages below approximately 0.25 mV. Heating can increase the measured capacitance at high bias voltages and heating effects were observed in one of the junctions measured. However, since the effects of heating and the substrate could be observed in the measurement it was possible to eliminate them by using values of the measured capacitance in the regime where they had no effect. The effect of thermal noise on the measurement was assessed and is an order of magnitude less than the observed changes in capacitance. The grain boundary capacitance increased from 0.2 Fm^{-2} for $x=0$ to a maximum value of 1.2 Fm^{-2} for $x=0.3$. Due to the complex structure of the boundaries and in the absence of knowledge of how doping effects the dielectric constant, it is difficult to make definite conclusions about how these capacitance changes relate to changes in the boundary's electrical structure. However, the inverse relationship between capacitance per unit area and resistance area product is consistent with changes in the effective area of the boundary occurring as calcium is added.

ACKNOWLEDGMENTS

This work was supported by the E.P.S.R.C. (Cambridge), the European T.M.R. Supercurrent network (Cambridge), the D.A.A.D. (Augsburg), the B.M.B.I. (EKM 13N6918, Augsburg), and the D.F.G. (SFB 484, Augsburg). J.H.T.R. thanks Alex Gurevich, Juergen Halbritter, David Larbelestier, and John Lister for valuable discussions.

APPENDIX: A MODEL FOR HEATING IN HIGH T_c THIN FILM GRAIN BOUNDARY JUNCTIONS

A simple model for predicting the heating of a grain boundary junction is presented. It is assumed that the $YBa_2Cu_3O_{7-\delta}$ track across the grain boundary can be modeled as a one-dimensional system, and that heat loss occurs by flow of heat away from the grain boundary and into the substrate, which is treated as a heat bath at the same temperature as the surroundings. Heat flow from the track directly into the liquid helium can be neglected.[17] The system is assumed to be in thermal equilibrium on the time scale of the measurement.

Consider an element of the track at a distance x from the grain boundary. The temperature $T(x)$ is related to the heat current per unit area of the track by the equation

$$T(x+dx) = T(x) - \frac{1}{\kappa}J(x)dx, \quad \text{(A1)}$$

where κ is thermal conductivity of the track. The heat losses to the substrate, at temperature T_b, are governed by the equation

$$J(x+dx) = J(x) - \frac{\alpha(T-T_b)}{h}dx, \quad \text{(A2)}$$

where α is the heat transfer coefficient per unit area of the substrate /film boundary and h is the film thickness.

By eliminating $J(x)$ the following second order differential equation can be derived:

$$\frac{d^2T}{dx^2} = \frac{\alpha}{\kappa h}(T-T_b). \quad \text{(A3)}$$

If it is assumed that κ and α are temperature independent, this equation can be solved with the boundary conditions $T \to T_b$ as $x \to \infty$ and $J(0)=IV/(2hw)$, giving the solution

$$T = T_b + \sqrt{\frac{1}{\alpha h \kappa}}\frac{IV}{2w}\exp\left(-\sqrt{\frac{\alpha}{\kappa h}}x\right), \quad \text{(A4)}$$

where I is the current flowing through the track, V is the voltage dropped across the junction, and w is the width of the track.

However both α and κ are strong functions of temperature for $YBa_2Cu_3O_{7-\delta}$ on $SrTiO_3$, so this solution is only applicable if the temperature rises predicted are small compared to T_b. α is determined by the acoustic mismatch model at temperatures significantly less than the Debye temperature.[35] Because α will be affected by the microstructure of the film-substrate interface, it cannot be calculated precisely. Following Cheeke, Ettinger, and Hebral[35] we estimate $\alpha = T^3/B$. B can be calculated from the properties of the materials on either side of the boundary,[35] for $YBa_2Cu_3O_{7-\delta}$ on $SrTiO_3$ $B = 9.6\times 10^4$ m^2 K^4 W^{-1}. Between 0 K and 10 K the thermal conductivity of $YBa_2Cu_3O_{7-\delta}$ can be reasonably approximated by the empirical expression $\kappa = \kappa_0 T^2$, where $\kappa_0 \approx 0.17$ W m^{-1} K^{-3}.[36] Using these approximations we derive a second differential equation

$$\frac{d^2T}{dx^2} = \frac{1}{\kappa_0 B h}T(T-T_b). \quad \text{(A5)}$$

This equation can be solved (with the integrating factor dT/dx), to give

$$T = \frac{T_b}{2}\left(3\coth^2\left(D + \frac{x}{2}\sqrt{\frac{T_b}{\kappa_0 B h}} - 1\right)\right), \quad \text{(A6)}$$

where the boundary condition $T \to T_b$ as $x \to \infty$ is satisfied and the integration constant D can be eliminated using the additional boundary condition $J(0)=IV/(2hw)$.

Equation (A4) was used to calculate the temperature rises at 15 K in Table I, whilst Eq. (A6) was used to calculate the temperature rises at 4.2 K. In the latter case the constant D was determined by numerical solution of the equation resulting from the boundary condition on $J(0)$. The assumption of thermal equilibrium can be tested by calculating the time it would take to heat up a length of track comparable to the decay length, given the power input IV. In this case the time is of order 1 ns, in good agreement with experiment.[37] This is much less than the measurement time (of order 1 s) so thermal equilibrium is a valid assumption.

---

*Electronic address: jhtr2@cam.ac.uk; presently at Cambridge University, Nanoscience Centre, J. J. Thomson Avenue, Cambridge CB3 0FF, United Kingdom.

†Presently at SSA SoftSolutions GmbH, Unterkreuthweg 3, D-86444 Mhlhausen, Germany.

‡Presently at ifm electronic GmbH, Wiesentalstr. 40, 88074 Meckenbeuren, Germany.

§Presently at Low Temperature Division, Faculty of Applied Physics, University of Twente, P.O. Box 217, 7500 AE Enschede, The Netherlands.

[1] D. Dimos, P. Chaudhari, J. Mannhart, and F. K. Legoues, Phys. Rev. Lett. **61**, 219 (1988).

[2] H. Hilgenkamp and J. Mannhart, Rev. Mod. Phys. **74**, 485 (2002).

[3] A. Schmehl, B. Goetz, R. R. Schultz, C. W. Schneider, H. Bielefeldt, H. Hilgenkamp, and J. Mannhart, Europhys. Lett. **47**, 110 (1999).

[4] C. W. Schneider, R. R. Schultz, B. Goetz, A. Schmehl, H. Bielefeldt, H. Hilgenkamp, and J. Mannhart, Appl. Phys. Lett. **75**, 850 (1999).

[5] G. Hammerl, A. Schmehl, R. R. Schultz, B. Goetz, H. Bielefeldt, C. W. Schneider, H. Hilgenkamp, and J. Mannhart, Nature (London) **407**, 162 (2000).

[6] J. Mannhart and H. Hilgenkamp, Mater. Sci. Eng., B **56**, 77 (1998).

[7] Symposium Z-MRS Fall 2002, December 2002 (unpublished).

[8] D. Winkler, Y. M. Zhang, P. A. Nilsson, E. A. Stepantsov, and T. Claeson, Phys. Rev. Lett. **72**, 1260 (1994).

[9] A. Beck, A. Stenzel, O. M. Froehlich, R. Gerber, R. Gerdemann, L. Alff, B. Mayer, R. Gross, A. Marx, J. C. Villegier *et al.*, IEEE Trans. Appl. Supercond. **5**, 2192 (1995).

[10] Y. M. Zhang, D. Winkler, G. Brorsson, and T. Claeson, IEEE Trans. Appl. Supercond. **5**, 2200 (1995).

[11] K. Nakajima, K. Yokota, H. Myoren, J. Chen, and T. Yamashita, IEEE Trans. Appl. Supercond. **5**, 2861 (1995).

[12] E. J. Tarte, G. A. Wagner, R. E. Somekh, F. J. Baudenbacher, P. Berguis, and J. E. Evetts, IEEE Trans. Appl. Supercond. **11**, 3662 (1997).

[13] M. G. Medici, J. Elly, M. Razani, A. Gilabert, F. Schmidl, P. Seidel, A. Hoffmann, and I. K. Schuller, J. Supercond. **11**, 225 (1998).

[14] P. F. McBrien, E. J. Tarte, R. H. Hadfield, W. E. Booji, A. Moya, F. Kahlmann, M. G. Blamire, C. M. Pegrum, and E. J. Tarte, Physica C **339**, 88 (2000).

[15] E. J. Tarte, P. F. McBrien, E. I. Inglessi, F. Kahlmann, W. E. Booji, and M. G. Blamire, Physica B **284–288**, 628 (2000).

[16] E. J. Tarte, P. F. McBrien, J. H. T. Ransley, R. H. Hadfield, E. I. Inglessi, W. E. Booji, G. Burnell, and J. E. Evetts, IEEE Trans. Appl. Supercond. **11**, 418 (2001).
[17] W. J. Skocpol, M. R. Beasley, and M. Tinkham, J. Appl. Phys. **45**, 4054 (1974).
[18] T. A. Fulton and L. N. Dunkleberger, Phys. Rev. B **9**, 4760 (1974).
[19] D. E. McCumber, J. Appl. Phys. **39**, 3113 (1968).
[20] R. C. Neville, B. Hoeneisen, and C. A. Mead, J. Appl. Phys. **43**, 2124 (1972).
[21] R. C. Neville, B. Hoeneisen, and C. A. Mead, J. Appl. Phys. **43**, 3903 (1972).
[22] K. K. Likharev, *Dynamics of Josephson Junctions and Circuits* (Gordon and Breach, Amsterdam, 1986), Chaps. 1–5.
[23] H. A. Kramers, Physica (Amsterdam) **7**, 284 (1968).
[24] M. G. Castellano, R. Leoni, G. Torrioli, F. Chiarello, C. Cosmelli, A. Costanti, G. Diambrini-Palazzi, P. Carelli, R. Christiano, and L. Frunxio, J. Appl. Phys. **80**, 2922 (1996).
[25] J. R. Kirtley, C. D. Tesche, W. J. Gallagher, A. W. Kleinsasser, R. L. Sandstrom, S. I. Raider, and M. P. A. Fisher, Phys. Rev. Lett. **61**, 2372 (1988).
[26] M. G. Castellano, G. Torrioli, F. Chiarello, C. Cosmelli, and P. Carelli, J. Appl. Phys. **86**, 6405 (1999).
[27] Q. Jin and S.-W. Chan, J. Mater. Res. **17**, 323 (2002).
[28] N. D. Browning, J. P. Burban, C. Prouteau, G. Duscher, and S. J. Pennycook, Micron **30**, 425 (1999).
[29] C. Træholt, J. G. Wen, H. W. Zandbergen, Y. Shen, and J. W. M. Hilgenkamp, Physica C **230**, 425 (1994).
[30] J. L. Alarco, E. Olsson, Z. G. Ivanov, D. Winkler, E. A. Stepantsov, O. I. Lebedev, A. L. Vasiliev, and N. A. Kiselev, Physica C **247**, 263 (1993).
[31] S.-W. Chan, Q. Jin, J. W. H. Tsai, S. C. Tidrow, and Q. Jiang, IEEE Trans. Appl. Supercond. **13**, 2829 (2003).
[32] D. J. Miller, T. A. Roberts, J. H. Kang, J. Talvacchio, D. B. Cuchholz, and R. P. H. Chang, Appl. Phys. Lett. **66**, 2561 (1995).
[33] J. Mannhart, A. Kleinsasser, J. Strobel, and A. Baratoff, Physica C **216**, 401 (1993).
[34] B. Moeckly and R. A. Buhrman, Appl. Phys. Lett. **65**, 3126 (1994).
[35] J. D. N. Cheeke, H. Ettinger, and B. Hebral, Can. J. Phys. **54**, 1749 (1976).
[36] C. Uher, *Physical Properties of High Temperature Superconductors II* (World Scientific, Singapore, 1992).
[37] M. Nahum, S. Verghesse, P. L. Richards, and K. Char, Appl. Phys. Lett. **59**, 2034 (1991).